THE JOURNAL OF PHYSICAL CHEMISTRY A
A JOURNAL OF THE AMERICAN CHEMICAL SOCIETY

pubs.acs.org/JPCA Article

Gas-Phase Chlorine Radical Oxidation of Alkanes: Effects of Structural Branching, NO_x, and Relative Humidity Observed during Environmental Chamber Experiments

Leif G. Jahn, Dongyu S. Wang, Surya Venkatesh Dhulipala, and Lea Hildebrandt Ruiz*

Cite This: https://doi.org/10.1021/acs.jpca.1c03516 Read Online

ACCESS | Metrics & More | Article Recommendations | Supporting Information

ABSTRACT: Chlorine-initiated oxidation of alkanes has been shown to rapidly form secondary organic aerosol (SOA) at higher yields than OH−alkane reactions. However, the effects of the alkane volatile organic compound precursor structure and the reasons for the differences in SOA yield from OH−alkane reactions remain unclear. In this work, we investigated the effects of the alkane molecular structure on oxidation by the chlorine radical (Cl) and resulting formation of SOA through a series of laboratory chamber experiments, utilizing data from an iodide chemical ionization mass spectrometer and an aerosol chemical speciation monitor. Experiments were conducted with linear, branched, and branched cyclic C_{10} alkane precursors under different NO_x and RH conditions. Observed product fragmentation patterns during the oxidation of branched alkanes demonstrate the abstraction of primary hydrogens by Cl, confirming a key difference between OH- and Cl-initiated oxidation of alkanes and providing a possible explanation for higher SOA production from Cl-initiated oxidation. Low-NO_x conditions led to higher SOA production. SOA formed from butylcyclohexane under low NO_x conditions contained higher fractions of organic acids and lower volatility molecules that were less prone to oligomerization relative to decane SOA. Branched alkanes produced less SOA, and branched cycloalkanes produced more SOA than linear *n*-alkanes, consistent with past work on OH-initiated reactions. Overall, our work provides insights into the differences between Cl- and OH-initiated oxidation of alkanes of different structures and the potential significance of Cl as an atmospheric oxidant.

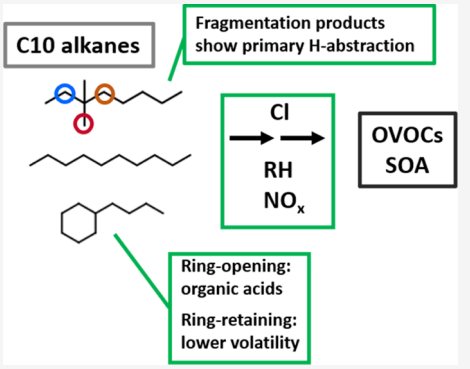

1. INTRODUCTION

Atmospheric chlorine radical (Cl) is an important atmospheric oxidant that is generally more reactive toward hydrogen abstraction than the hydroxyl radical (OH) but is present in lower concentrations and in more limited regions of the atmosphere.[1−5] Cl has long been understood to originate from marine sea spray aerosol[6] as well as a variety of natural and anthropogenic sources that have been summarized previously.[1,7,8] Ambient measurements have suggested additional sources of Cl through observations in a variety of inland regions.[7,9,10] A number of recent studies have identified diverse and potentially significant sources for atmospheric chlorine radicals, including biomass-burning aerosol,[11,12] playa and lakebed dust,[13] and road salt.[14] Given the varied known sources and mechanisms for Cl production and the potential for yet-uncharacterized sources, understanding the oxidative chemistry of Cl and volatile organic compounds (VOCs) is important for obtaining accurate model predictions for the production of secondary pollutants including secondary organic aerosol (SOA) and ozone.[15]

The reactions of Cl with a variety of VOCs have a higher rate constant[3,4] and can result in higher SOA yields than reactions with OH.[1,16,17] One particularly important class of VOC in this context appears to be alkane hydrocarbons[1] due to a substantially higher reaction rate with Cl compared to OH.[3,18] Alkanes comprise a significant portion of urban VOCs, originating from varied sources such as combustion and vehicle emissions,[19−21] asphalt usage,[22] and commercial products and activities (e.g., cleaning and personal care products).[23,24] Alkanes are also present in non-urban areas and have been linked to upstream fossil fuel processes.[25−27] Recent experimental work has shown higher yields of SOA from the high-NO_x oxidation of linear C8−C12 alkanes by Cl relative to oxidation by OH.[1] The increased yield was theorized to result from the ability of chlorine radicals to abstract hydrogen atoms from terminal carbon groups leading to the formation of alkanes with terminal substituents,[1] which was based on prior measurements and structure−activity predictions.[3] In contrast, the hydroxyl radical is not predicted and has not been observed

Received: April 20, 2021
Revised: July 27, 2021

Table 1. List of Experiments with Initial Conditions and Summary of Results

expt. #	hydrocarbon precursor	RH	NO[b]	NO_2[b]	SOA conc.[c,d]	yield[d]	f_{43}[c]	f_{44}[c]
1	decane[a]	<5%	32	0	59	0.81	8.4×10^{-2}	1.0×10^{-1}
2	decane	<5%	36	0	69	0.95	8.5×10^{-2}	9.9×10^{-2}
3	decane[a]	<5%	19	18	63	0.86	8.1×10^{-2}	1.3×10^{-1}
4	decane	<5%	0	0	98	1.34	9.0×10^{-2}	7.5×10^{-2}
5	decane	~40%	0	0	120	1.63	9.0×10^{-2}	7.6×10^{-2}
6	decane	~55%	0	0	160	2.16	9.8×10^{-2}	6.6×10^{-2}
7	decane[a]	~40%	19	17	37	0.51	8.6×10^{-2}	8.6×10^{-2}
8	butylcyclohexane (BCH)	<5%	36	2	77	0.94	6.5×10^{-2}	1.1×10^{-1}
9	butylcyclohexane (BCH)	<5%	18	1	92	1.12	6.1×10^{-2}	1.1×10^{-1}
10	butylcyclohexane (BCH)	<5%	0	0	140	1.70	7.1×10^{-2}	1.1×10^{-1}
11	butylcyclohexane (BCH)	~50%	0	0	140	1.70	6.3×10^{-2}	9.6×10^{-2}
12	2-methylnonane (2-MeNo)	<5%	35	0	44	0.61	8.9×10^{-2}	1.2×10^{-1}
13	3,3-dimethyloctane (3,3-DMO)	<5%	38	0	16	0.22	9.3×10^{-2}	1.3×10^{-1}

[a]Experiments previously described in Wang and Hildebrandt Ruiz (2018). [b]Measured in ppb (volume). [c]SOA concentration, f_{43}, and f_{44} are derived from ACSM measurements and are 15 min averages taken after a maximum organic concentration is reached. [d]Yield is calculated based on the SOA concentration and the initial precursor concentration.

to abstract terminal hydrogens to a significant extent from medium- and long-chain alkanes.[28,29] Substituents located at or near the end of an alkane will increase SOA yields both by directly lowering alkane vapor pressure[30−32] and by directing subsequent oxidation chemistry in a manner that disfavors fragmentation to less volatile products.[28,33,34]

Emitted alkanes possess a variety of molecular structures, including linear, branched, cyclic, and branched cyclic structures.[19,22,25] Alkane structure can have a substantial impact on how oxidation chemistry proceeds and how much SOA forms.[35−37] Relative to a base scenario where a linear alkane is oxidized under high-NO_x conditions, cyclic alkanes of comparable carbon number produce more SOA because alkoxy radical (RO) decomposition and bond scission can lead to a ring-opening reaction that produces an aldehyde and primary carbon radical while preserving the number of carbons in the molecule.[37] In contrast, branched alkanes produce less SOA because bond scission leading to molecular fragmentation and the production of more volatile smaller carbon number molecules tends to be more favorable, as fragmentation near a branching point will produce a more stable substituted carbon radical.[35,36] Branched cycloalkanes have a less generalizable trend for SOA formation compared to cyclic and branched alkanes,[36] as their oxidation chemistry contains aspects of both cyclic and branched alkanes.[37,38] Most prior studies were conducted under high-NO_x conditions with the hydroxyl (OH) radical as the oxidant. The effects of alkane structure under low and high-NO_x conditions on chlorine oxidation chemistry have not been investigated experimentally, and potentially unique contributions of Cl chemistry to VOC oxidation and SOA formation are difficult to discern during ambient measurements.[39] Instead of extrapolating from established OH−akane chemistry, which has been shown to differ from chlorine-alkane chemistry, a more detailed experimental understanding of Cl as an oxidant and the effects of structural branching on alkane oxidation will better aid in the development of accurate estimations of VOC oxidation and SOA production. Here, we present results from a series of laboratory chamber experiments on Cl-initiated oxidation of linear, branched, and branched cyclic C10 alkane precursors to assess the effects of NO_x and RH on the oxidative chemistry and SOA formation potential for each of these alkane structures.

2. EXPERIMENTAL METHODS

Experiments were conducted in an environmental chamber consisting of a 10 m^3 Teflon bag surrounded by UVA blacklights (general #32085, ~354 nm) and supplied with clean air from a zero air generator (Aadco 737R). Prior to turning on the UV lights, ammonium sulfate seed aerosol was injected from an aqueous ammonium sulfate solution (0.01 M) using an aerosol generation system (Brechtel AGS 2002). Precursor gasses Cl_2 (101 ppm in N_2, Airgas) and NO and/or NO_2 (Airgas 9.98 and 9.86 ppm in N_2, respectively) were injected from gas cylinders and controlled using mass flow controllers (Alicat). The VOC precursors, *n*-decane, 2-methylnonane, 3,3-dimethyloctane, and butylcyclohexane were purchased in the liquid form (Sigma-Aldrich, CAS #'s 124-18-5, 871-83-0, 41110-44-5, and 1678-93-9, respectively). These are abbreviated as decane, 2-MeNo, 3,3-DMO, and BCH through the rest of the paper. An initial Cl_2 concentration of 40 ppb (volume) was used in each experiment. Laboratory experiments utilizing high oxidant exposure may enable reactions that are not common under ambient conditions,[40] for example, reactions of RO_2 radicals with OH or Cl.[40−42] However, chamber modeling for gas-phase alkane−Cl chemistry in the SAPRC framework using the Carbon Bond Mechanism (CB6r4, see Supporting Information, Section S1, for details of the modelling work) suggests that NO or HO_2 concentrations remained sufficiently high[40] over the course of experiments such that RO_2 + Cl/OH was not a substantial loss process (Figure S1). NO and NO_2 concentrations were measured throughout the experiment with a chemiluminescence monitor (Teledyne 200E) and a cavity attenuated phase shift NO_2 analyzer (CAPS-NO_2, Environment S.A. A32M). NO concentrations were typically depleted to below the detection limit within ~10 min after lights were turned on, while NO_2 concentrations initially spiked as lights were turned on and then decreased before plateauing for the duration of the experiment (Figure S1a). The chamber may contain some amount of residual NO_x during low-NO_x experiments; however, a lack of substantial organonitrate formation suggests that NO_x levels were not sufficient to significantly affect oxidation chemistry during low-NO_x experiments. VOCs were introduced to the chamber via a 250 mL glass sampling tube (Kimble Chase) with a 2 L min^{-1} flow of lightly heated zero air. 1 μL of each VOC precursor was injected for each

https://doi.org/10.1021/acs.jpca.1c03516
J. Phys. Chem. A XXXX, XXX, XXX−XXX

experiment leading to precursor volume concentrations of 11 ppb (decane, 2-MeNO, and 3,3-DMO) and 13 ppb (BCH); mass concentrations were 73 and 82 $\mu g\ m^{-3}$, respectively. After the reactants were well-mixed in the chamber, UV lights were turned on to initiate oxidation, which is the time designated as the start of each experiment and remained on for 30−60 min. Chamber modeling suggests that the parent VOC is consumed within approximately 10 min.[43,44]

Aerosol size distributions were monitored with a scanning electrical mobility spectrometer (Brechtel 2002). Bulk particle composition was measured with an aerosol chemical speciation monitor (Ng et al. 2011; ACSM, Aerodyne) that was calibrated as described previously.[1] ACSM data analysis was conducted in Igor (version 6.37, Wavemetrics Inc.) using ACSM local 1.6.1.0 (Aerodyne). SOA concentrations were calculated using ACSM measurements while assuming a collection efficiency of 0.5 and a relative ionization efficiency of 1.4 for organics. SOA was calculated as the sum of the ACSM-measured organic and nitrate fragments to account for the formation of organonitrate molecules. Wall-loss corrections were performed according to the method described in Pathak et al. (2007). Wall losses of gas-phase molecules were not accounted for which may bias measured SOA yields low, but such losses are not expected to substantially impact yield calculations over the timeline during which SOA concentrations are measured (~30 min since start of photo-oxidation; see Table 1).[45] Gas-phase composition was measured with a high-resolution time-of-flight chemical ionization mass spectrometer with I^- reagent ionization (Aerodyne; hereafter referred to as I^- CIMS or CIMS). The I^- CIMS has been described in detail in prior publications.[16,46] A filter inlet for gases and aerosols (FIGAERO) was also used with the I^- CIMS to analyze particle composition, which has also been described in prior work.[1,46,47] In brief, the FIGAERO system (FIGAERO-CIMS) alternates between gas-sampling/particle-collection and particle-sampling mode. During gas-sampling/particle-collection mode, the sample flow was pulled through a 2.0 μm pore-size PTFE filter (Pall Corporation Zefluor, 24 mm) at 3 SLPM to collect particles on the filter while gas sampling was conducted through a parallel sampling line. Particle collection lasted 15−45 min during each experiment. During particle-desorption mode, a heated flow of clean air or ultra-high purity N_2 was passed through the filter to volatilize compounds from the collected particles for analysis by the CIMS. Flow was heated from 25 to 200 °C (as measured just above the filter) at 10 °C min^{-1} for an ~20 min desorption cycle which was then followed by a 20 min soaking period at 200 °C to desorb remaining material. The signal measured by the CIMS between 25 °C (room temperature) and 180 °C is then plotted against the gas temperature to create a thermogram (see Figure 4). Data analysis was conducted using Igor Pro 6.7.3.2 (Wavemetrics) with Tofware versions 2.5.13 (Tofware; CIMS) or 2.5.11 (FIGAERO-CIMS). A uniform response factor by the I^- CIMS to analyte molecules is assumed.[48]

3. RESULTS AND DISCUSSION

Table 1 summarizes conditions of the chamber experiments discussed in this work. Also shown in Table 1 are ACSM-derived SOA measurements, which are discussed in more detail in Section 3.4. Characterization of gas- and particle-phase alkane oxidation products and the relevance of these measurements to the observed SOA trends are discussed in Sections 3.1−3.3.

A significant difference between the oxidation of alkanes by Cl and OH is the greater propensity for Cl to abstract primary H. We have estimated, in a manner consistent with past work[33,49] and based on previously determined structure activity relationships,[3] the percentage of initial H abstraction that occurs at primary sites in each parent VOC used in this work, as well as the percentage at other sites. These estimates are compiled for each unique precursor H-abstraction site in Table 2 below and are outlined in greater detail in Supporting Information, Section S2. Chemically distinct sites that have the same H abstraction rate are grouped together in the table; for example, the H abstraction rates for the carbon 1, carbon 8, and methyl group primary sites within 3,3-DMO are grouped together to give the 27% value. Percentages for oxidation by OH are calculated in the same manner[29] and shown in parentheses, illustrating differences in where initial H abstraction occurs from the two oxidants. Cl is more likely to abstract H from near the end of an alkyl chain (primary and primary-adjacent sites), while OH is more likely to abstract from tertiary sites.

Table 2. Percentage of Initial H-Abstraction Occurring at the Different Unique Sites within Each of the Precursor VOCs Used in This Work[a]

	n-decane	BCH	3,3-DMO	2-MeNo
primary (secondary)[b]	11% (3)[c]	5% (1)	27% (9)	17% (4)
secondary (primary + secondary)	27% (21)	14% (8)	34% (32)	15% (10)
secondary (secondary + secondary/tertiary/quaternary)	63% (76)	75% (67)	40% (59)	57% (64)
tertiary (primary + primary + secondary)	n/a	n/a	n/a	11% (22)
tertiary (secondary + secondary + secondary)	n/a	6% (24)	n/a	n/a

[a]Percentages may add to >100% due to rounding. [b]Substitution of adjacent carbon sites is indicated in parentheses. [c]Values shown are for Cl (and OH in parentheses).

3.1. Effects of Branching: Insights from 3,3-Dimethyloctane. Analysis of the gas- and particle-phase compositions of 3,3-DMO and decane oxidation products provides insight on the effects of branching and alkane oxidation in general. The simplest C10 products observed are di-substituted alkanes that contain a nitrate group, either second-generation dinitrates or first-generation 1,4-hydroxynitrates, consistent with prior work and known mechanisms on the OH-initiated oxidation of alkanes.[35,50] Several early generation alkane oxidation products such as C10 mononitrate or hydroxy−ketone molecules[35] are not effectively detected by the I^- CIMS. The signal for hydroxynitrates rises before the signal for dinitrates (Figure S3), consistent with their formation during the first generation of oxidation. Other second generation products such as C10 ketone−hydroxy−nitrate and C10 ketone−ketone−nitrate are detected shortly after C10 dinitrate (Figure S3).

The main difference in the oxidation chemistry between decane and 3,3-DMO is the increased propensity for fragmentation in 3,3-DMO following initial H-abstraction. Fragmentation of the parent 3,3-DMO is expected to be favorable following H-abstraction at carbon-2, carbon-4, or either of the methyl substituents. This is illustrated in Schemes

https://doi.org/10.1021/acs.jpca.1c03516
J. Phys. Chem. A XXXX, XXX, XXX−XXX

Scheme 1. Formation of 1,4 Hydroxynitrates from the Oxidation of 3,3-DMO under High-NO_x Conditions[a]

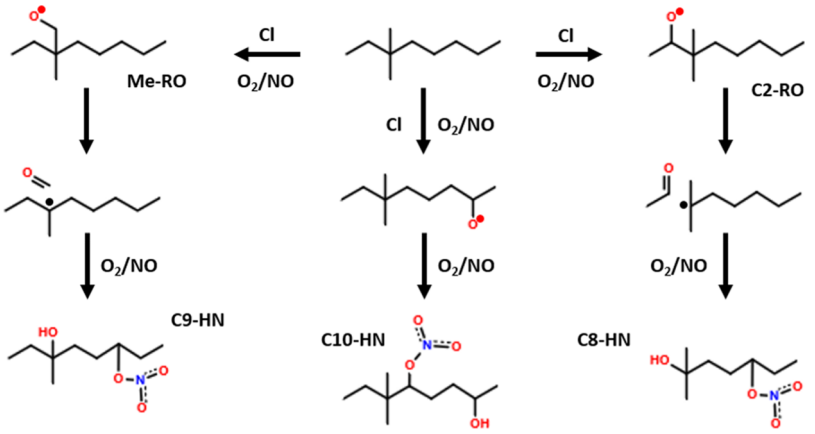

[a]Shown are potential reaction pathways following initial H-abstraction at carbon-2, the primary methyl groups, and carbon-7. Abstraction at the methyl position and at carbon-2 are expected to be the main pathways that form the C9 and C8 hydroxynitrate molecules, respectively. A more detailed scheme is shown in Scheme S1. The C10 nitrate molecule can form after abstraction if molecular decomposition does not occur (which is likely for most remaining positions). The middle and right-side branches are expected to be similar to oxidation by OH, while the left-side branch is expected to be more significant for oxidation by Cl.

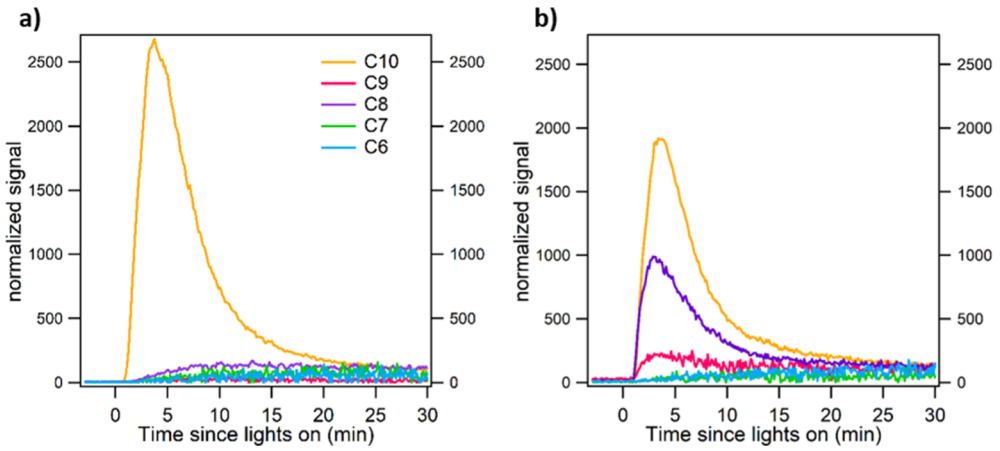

Figure 1. Gas-phase I^- CIMS timeseries for C6-10 hydroxynitrate ($C_xH_{2x+1}ONO_3$) molecules formed during the high NO_x oxidation of decane [(a) expt. 1] and 3,3-DMO [(b) expt. 13]. Signals have been averaged over 7.5 s timescales and normalized to an I^- signal of 1×10^6.

s1 1 and S1 (provided in Supporting Information) and leads to the formation of an aldehyde and tertiary carbon radical through previously described mechanisms.[50] This is a relatively favorable process compared to fragmentation after H-abstraction at any carbon atom on *n*-decane as this would form a primary carbon radical.[50] The extent of fragmentation following initial oxidation can be tracked through the signals for several of the reaction products discussed above. We focus primarily on the 1,4-hydroxynitrates $C_xH_yOHNO_3$ (abbreviated as CX-HN) during this discussion, as it is the simplest first-generation product we can detect. We assume uniform ionization efficiency by the I^- CIMS of the C6−C10-HN f1 molecules. Figure 1 compares the ion intensities of C6−C10-HN molecules which form either following the initial oxidation of the alkane (C10-HN) or after initial oxidation leads to fragmentation and the formation of a C < 10 alkyl radical.[35] These reactions are shown in Schemes 1 and S1. The C10-HN signal during decane oxidation is much more intense than that of C(6−9)-HN. This is expected, as there are no favorable locations for fragmentation to occur within the molecule. In contrast, there are clear indications of C8- and C9-HN production during 3,3-DMO oxidation (Figure 1b), which corresponds to the left and right branches of the reaction scheme illustrated in Scheme 1, while C6-HN and C7-HN production remain negligible, which would be expected from the proposed main oxidation pathways.

The suggested formation pathway for each of the detected molecules is shown in Scheme 1. C9-HN is proposed to form following H-abstraction at one of the substituent methyl groups, as no other reasonable pathway is apparent. This C9-HN pathway is expected to be more prevalent during oxidation by Cl, while the pathways to form C10-HN and C8-HN would be expected to occur during OH oxidation as well. Approximately 13% of initial H-abstraction in 3,3-DMO is expected to occur at the methyl positions, estimated based on previously described structure−activity relationships; the estimated proportion of H-abstraction occurring at each site for the molecules used in this work is listed in Table 2.[3] The present experimental observations are consistent with previous structure−activity predictions that Cl will abstract primary H atoms during oxidation of medium- and long-chain alkanes,[3] in contrast to negligible primary-H abstraction during OH-radical oxidation.[29] The lower intensity of the C9-HN signal compared to the C8-HN is due to a higher percentage of

https://doi.org/10.1021/acs.jpca.1c03516
J. Phys. Chem. A XXXX, XXX, XXX−XXX

initial H abstraction occurring at carbon 2 (~17%) and differing branching ratios between isomerization and decomposition at the two sites. Decomposition of the methyl group primary alkoxy radical (structure Me-RO in Scheme 1) is expected to occur to a lesser extent than decomposition of the secondary alkoxy radical at carbon 2 (structure C2-RO).[49,51] The abstraction rate for the primary H at the methyl groups may differ from that at the terminal primary H under some conditions due to the different local bonding environments for the carbon atoms: the methyl group C is bound to a quaternary C, while the terminal C is bound to a secondary C.[52] However, at room temperature, the abstraction rates by Cl are predicted to be identical.[3,53] Abstraction rates of the two types of primary H by OH are also estimated and predicted to be nearly identical,[29,52] offering support that the rates should be nearly identical for abstraction by Cl as well.

Fragmentation of 3,3-DMO would also be expected to occur following H-abstraction at carbon-5, producing 1-pentanal and the alkyl radical 2-methylpentane (with the radical on carbon-2). Formation of the 1,4-hydroxynitrate from the 2-methylpentane radical is less favorable than for the fragmentation products discussed above as the only H available for an internal 1,4-rearrangement are primary, which is less favorable than from a secondary or tertiary carbon. However, fragmentation to the C5 product can still be observed using the signal from the second-generation dinitrate product $C_{5-10}H_{10-20}(NO_3)_2$, abbreviated as CX-NN; we also assume uniform ionization efficiency for the C6-C10-NN molecules. The formation of a dinitrate product is outlined in Scheme S2 and entails the initial formation of an organonitrate and then subsequent oxidation and formation of a second nitrate group[35] and was observed during prior work.[1] Dinitrate products can form from each of the fragmentation products discussed above and the signals for these molecules are shown in Figure S4. The observed signal intensities for the C6-C10 dinitrates follow a similar trend as the C6-C10 hydroxynitrates, where C9-NN is less intense than C8-NN and C(6−7)-NN are mostly absent. The C5-NN signal is also less intense than C8-NN, likely due to the deactivating effect that the initial nitrate group has on second-generation abstraction at α and β carbons[28,29] and the overall higher number of abstractable H in the C8-N molecule compared to C5-N. Nitrate-group deactivation toward further H-abstraction and the potential for additional production during later-generation chemistry are likely why the C8-NN signal decays at a slower rate than C10-NN, assuming uniform sensitivity among the different dinitrate molecules.

C5-NN reaches a maximum concentration at a similar time as C(8−10)-NN but does not significantly decay over the time period examined in this experiment. C5-NN is volatile and unlikely to partition to the particle phase, and after the addition of two nitrate groups, each remaining abstractable hydrogen is α or β to a nitrate group and/or located on a primary carbon, rendering further H-abstraction relatively slow. This observation also illustrates another mechanism by which high-NO_x conditions may suppress SOA production. Smaller alkanes that form through molecular fragmentation will require the addition of a relatively larger number of functional groups to reach low enough vapor pressure to condense to the particle phase. A nitrate group may reduce the volatility of a molecule by comparable or greater amount compared to other common functional groups,[31,32,54] however if the addition of nitrate groups also inhibits the molecule toward further oxidation or internal H-shift, then speciation to nitrate groups (as opposed to other functional groups) may ultimately cause a molecule to remain relatively more volatile. This is a factor which likely becomes less relevant for SOA production as the chain length of the parent alkane increases, as longer chains and larger fragmentation products will have a lower initial volatility and more potentially abstractable H that are not impacted by nearby nitrate groups.

The tendency toward more fragmentation during oxidation of 3,3-DMO is also visible in the particle-phase FIGAERO measurements, where functionalized C < 10 molecules are relatively more abundant compared to C10 molecules for 3,3-DMO compared to decane. The average mass spectra during desorption for decane (red) and 3,3-DMO (blue) are shown in Figure S5. 3,3-DMO SOA was collected for 45 min compared to 15 min for decane SOA, resulting in similar overall intensities after normalization for the two experiments, even though 3,3-DMO formed less SOA. Differences are visible primarily when comparing the relative peak intensities of functionalized C < 10 molecules, which fall outside the repeating clusters of peaks that correspond to C10 families of molecules. The mono- and dinitrate $C_{10}H_yO_{3-5}(NO_3)$ and $C_{10}H_yO_{2-5}(NO_3)_2$ families are visible in Figure S5 as repeating and relatively intense peak clusters, with the locations of several families marked on the spectrum above the peak cluster. These molecules are the most common within the particle-phase and are present at comparable signal intensities between the decane and 3,3-DMO spectra. The m/z regions between these peak clusters are populated by signals from functionalized C < 10 molecules (<~430 m/z) and C11−15 oligomers (>~440 m/z), which are relatively more intense in 3,3-DMO SOA. The increased prevalence of C11−C15 oligomers in 3,3-DMO SOA follows from the increased production of C < 10 molecules that serve as precursors to these low-molecular weight oligomers. Also more pronounced in the spectrum of 3,3-DMO are peaks due to ammonium sulfate decomposition at m/z 391 and 403, which are likely enhanced due to the longer particle collection time and higher ammonium sulfate loading on the filter during the 3,3-DMO chamber experiment. C < 10 molecules are formed in both experiments as decomposition of an alkoxy radical becomes more likely as the alkane becomes more functionalized.[35,49]

3.2. Gas-phase Oxidation of Butylcyclohexane. The presence of the ring structure in BCH is expected to affect how oxidation proceeds compared to decane. There are six sites for H-abstraction (four unique) within the cyclohexyl ring of BCH. Alkoxy radicals that form on the ring can undergo bimolecular reaction with O_2 to form a carbonyl group, bond scission to form ring-opened products, or potentially internal isomerization. Prior work examining the oxidation of cyclic and polycyclic C10 alkanes by OH observed ring-opening processes to be significant in affecting oxidation and SOA formation;[37] however, ring opening may be relatively less significant for BCH due to the length and flexibility of the butyl substituent. The rigidity of the ring in the unsubstituted C6 cyclohexane prevents any internal isomerization by the alkoxy radical,[49] but the butyl substituent in BCH is flexible and may enable internal isomerization to occur from some of the carbon atoms within the hexyl ring, particularly those adjacent to the branching point. The rate at which alkoxy radical isomerization may occur from positions on the ring is unknown, which precludes an estimation of the extent to which each of these processes occur during the first generation of

https://doi.org/10.1021/acs.jpca.1c03516
J. Phys. Chem. A XXXX, XXX, XXX−XXX

Scheme 2. Ring Opening in Butylcyclohexane Following H-Abstraction para to the Butyl Substituent[a]

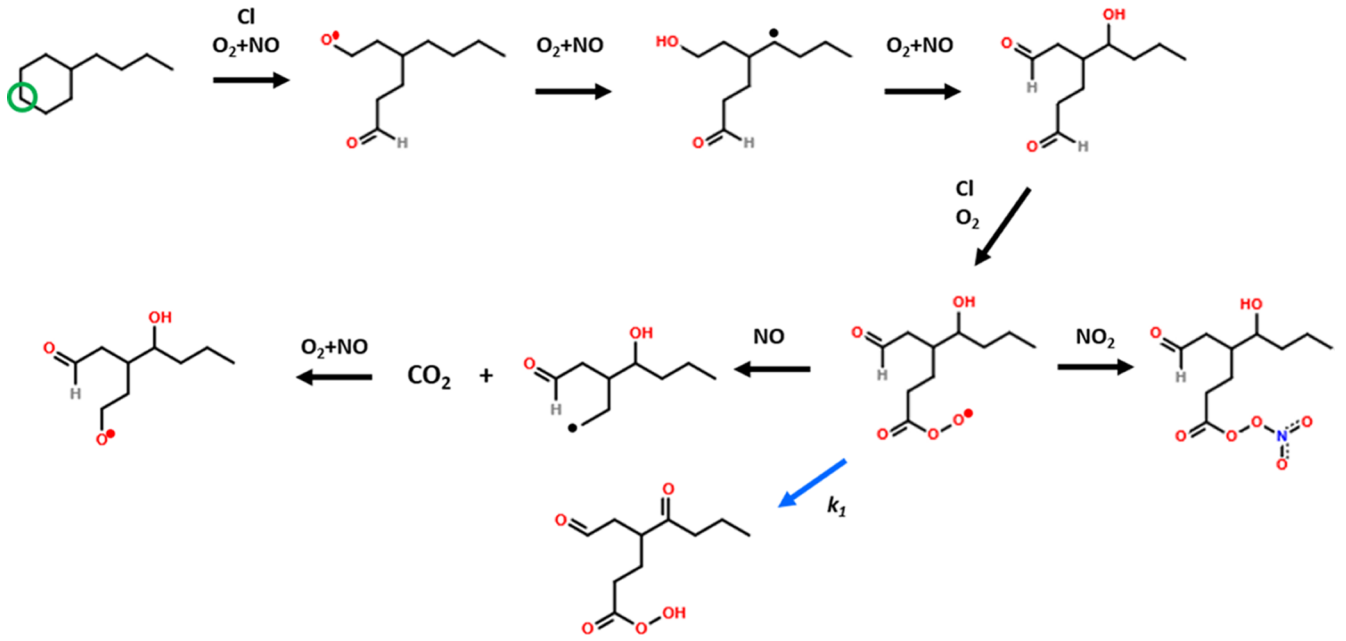

[a]The expected main product is a substituted di-aldehyde, similar to the previously described oxidation of cyclohexane.[56] The scheme shown here is not exhaustive and does not show a number of other potential reactions, which proceed through similar pathways to products of different structures. The rate k_1 marked with a blue arrow is not well-characterized and is discussed further in the main text.

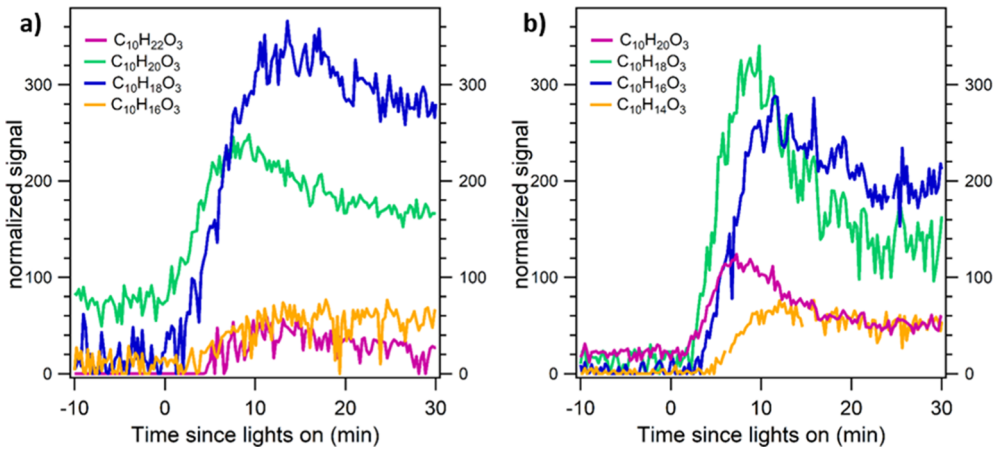

Figure 2. Gas-phase I^- CIMS timeseries for the $C_{10}H_xO_3$ molecules detected during low-NO_x oxidation of decane [(a) expt. 6] and BCH [(b) expt. 11]. Signals have been averaged over 15 s timescales. The values for "x" vary from 16−22 for decane and 14−20 for BCH, corresponding to 0−6 net H lost. Traces are colored according to the net number of H lost from the parent molecule.

oxidation. For the discussion in this work, we assume that alkoxy radicals formed at the para and meta positions on the hexyl ring (relative to the butyl substituent) will not undergo internal isomerization to a significant extent due to their greater distance from the flexible butyl substituent. Based on the structure of BCH, it appears reasonable that an alkoxy radical at the ortho position could form a six-membered transition state with the butyl substituent to undergo a 1,6 isomerization; however, an isomerization occurring from an alkoxy radical at the meta or para positions would necessitate a larger and more energetically unfavorable transition state;[55] we are unaware of prior work directly examining isomerization in cycloalkane structures. Ring opening is therefore more likely to occur when initial H abstraction occurs at the para and meta positions on the hexyl ring, which are estimated to be ∼32% of initial H-abstraction (Table 2). Based on the relative rates for reaction with O_2 and ring opening in cyclohexane, we expect approximately 60% of alkoxy radicals at the para and meta positions to result in first-generation ring opening.

The ring-opening process in BCH is shown in Scheme 2 for H abstraction occurring at the para position, which is expected to be similar to H abstraction at the meta position. Ring opening initially produces an aldehyde and a primary carbon radical, which reacts to produce a hydroxy−dialdehyde or organonitrate in the presence of NO.[37,56] Second-generation oxidation can abstract an H from many locations on the ring-opened molecule with abstraction of an aldehyde H likely.[29] This initially forms an acyl radical, which may decompose to produce CO and a primary carbon radical but will likely react with O_2 to form an acyl peroxy radical.[57] The acyl peroxy radical reacts with NO_2 to form a peroxyacyl nitrate or NO to form an acyloxy radical, which is expected to quickly

https://doi.org/10.1021/acs.jpca.1c03516
J. Phys. Chem. A XXXX, XXX, XXX−XXX

Scheme 3. Reaction Scheme Leading to the Formation of the Two Proposed Possible Structures for the $C_{10}H_{20}O_3$ Molecule Detected during BCH Oxidation, Marked as (1) and (2)[a]

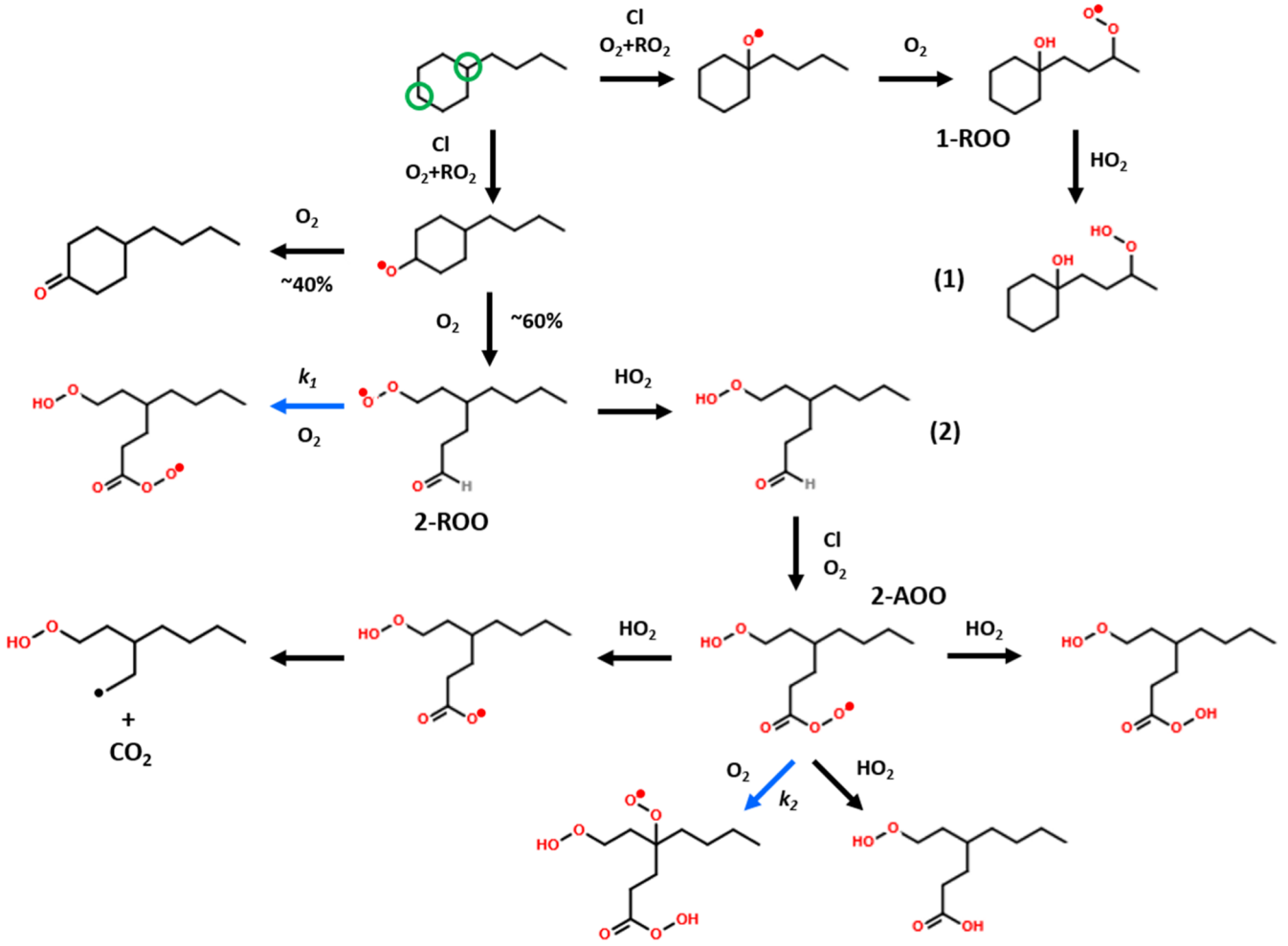

[a]Second-generation chemistry for structure 2 is also shown for abstraction occurring at an aldehyde group, with the isomerization rate k_2 estimated to be ~0.5 s^{-1}.[59] An estimate for the isomerization rate k_1 has not been calculated, though shorter aldehydic H shifts generally occur at rates on the order of 1 s^{-1}.[59]

decompose to CO_2 and a primary carbon radical.[51] The acyl peroxy radical may also undergo a 1,7 H-isomerization with a rate of k_1, marked by the blue arrow in Scheme 2. This rearrangement—a tertiary α-OH hydrogen to an acyl peroxy radical—may occur at a rate that is competitive with bimolecular reactions even under high NO_x conditions.[58,59] 1,5 or 1,6 H-isomerizations from the α-OH carbon are available to the acyloxy radicals that form following H-abstraction at either aldehyde group and have also been calculated to have a low energy barrier.[55] We do not show this pathway in Scheme 2 as it is not directly observed, and quantum chemical calculations suggest it is not likely to be significant,[51,55] but we mention the possibility as modeling the behavior of the acyloxy radical has been described as complex[51] and recent work has highlighted a gap in the mechanistic understanding of how oxidation proceeds in similarly structured molecules.[60]

The formation of first-generation ring-opened products can be observed through the gas-phase I^- CIMS data. Ring opening is expected to occur more frequently under high-NO_x conditions due to increased formation of alkoxy radicals. However, high-NO_x conditions also provide more pathways for propagation of the radical reaction sequence, so ring-opened products are initially easier to track under low-NO_x conditions. Figure 2 shows gas-phase signals for four potential early generation oxidation products of BCH and decane (under low-NO_x) that contain three O atoms; molecules containing two or fewer O atoms are not consistently detected. The traces are colored according to the number of H atoms lost from the parent molecule and show that BCH is unique from decane in that one of the detected compounds has lost a net of zero H atoms while adding three O. The production of, presumably, a first-generation hydroxy-hydroperoxide or aldehyde-peroxide appears to be unique to BCH (i.e., $C_{10}H_{20} \rightarrow C_{10}H_{20}O_3$) and is depicted in Scheme 3. The fact that comparable oxidation products are not observed during decane oxidation suggests that other reaction pathways are not responsible for the formation of this molecule. Structure 1, as depicted in Scheme 3, is a hydroxy-hydroperoxy molecule that may form if initial H-abstraction occurs at the branch point on the ring, while structure 2 is a ring-opened molecule containing an aldehyde functionality and a hydroperoxy group. Both of these structures are likely feasible; however, we would expect that most of the signal is due to structure 2 (Scheme 3). Only ~6% of the initial

https://doi.org/10.1021/acs.jpca.1c03516
J. Phys. Chem. A XXXX, XXX, XXX−XXX

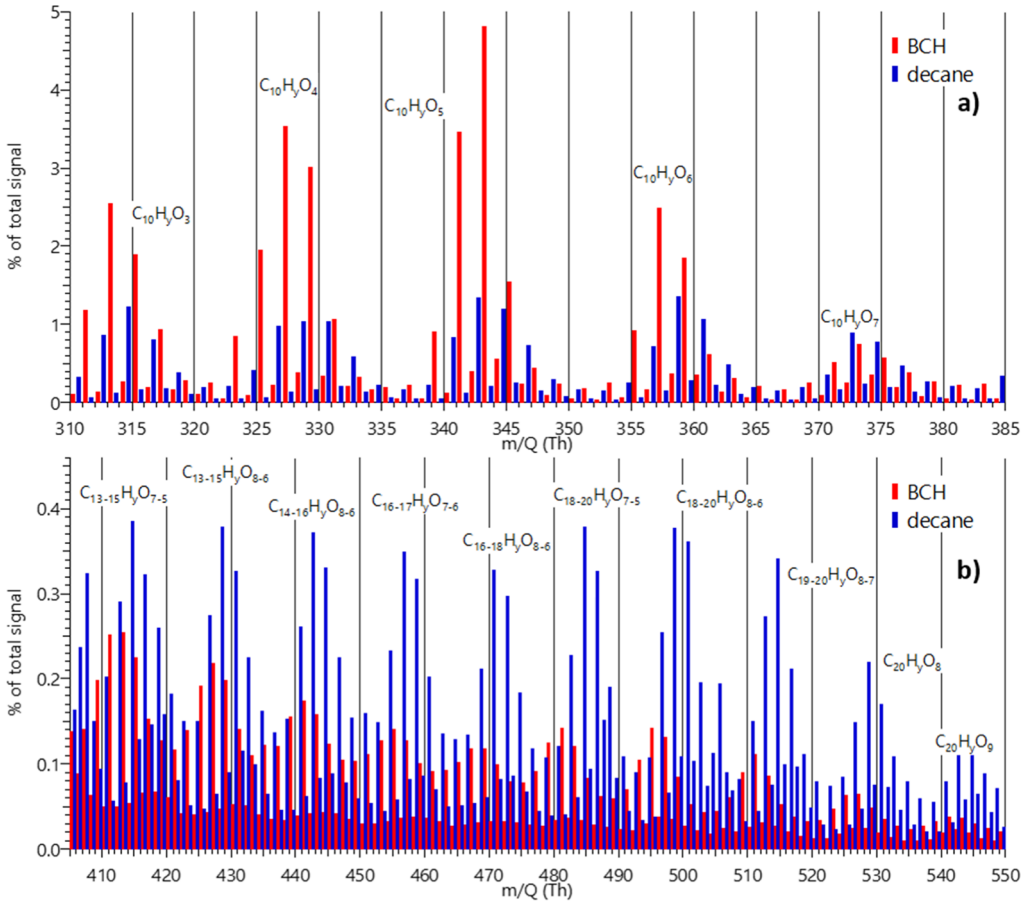

Figure 3. Average I^- FIGAERO-CIMS mass spectra for decane (blue, expt. 6) and BCH (red, expt. 11) low-NO_x SOA during the FIGAERO desorption cycle. Signals at each m/z are plotted as their percent of the total organic signal (total signal minus reagent ion and decomposition of ammonium sulfate seed aerosol) measured during the desorption cycle. The upper spectrum (a) shows the m/z range comprising C10 monomers, while the lower spectrum (b) shows the m/z range comprising some of the dimers and oligomers. Selected C10 and C > 10 molecular families are annotated. Monomer signals compose a larger fraction of BCH SOA, while oligomer and dimer signals compose a larger fraction of decane SOA. In (a), most of the intense peaks in the spectrum are offset by 2 m/z, corresponding to the 2 a.u. difference between decane and BCH. In (b), most of the intense peaks are offset by 2−4 m/z, reflecting a mix of ring-retaining and ring-opened BCH molecules. HOMs with O/C > 0.5 are observed in SOA originating from both alkane precursors.

H abstraction on BCH is estimated to occur from the tertiary site (Table 1) in contrast to ∼32% occurring from the meta and para positions on the hexyl ring. After a peroxy radical forms at one of these positions, reaction with RO_2 will compete with other reaction channels, primarily HO_2 but also potentially OH and Cl.[40−42] The RO_2−RO_2 reaction rate of the tertiary RO_2 would be approximately an order of magnitude lower than the reaction rate of the secondary RO_2,[49,61] indicating that the tertiary RO_2 will be more likely to react along a different pathway than shown in Scheme 3. Internal isomerization of the peroxy radicals 1-ROO and 2-ROO, shown in Scheme 3, are also possible. Isomerization of 1-ROO is estimated to be quite slow due to the OH group β to available carbons,[59] while isomerization of 2-ROO may be competitive under some conditions. This would be a 1,8 shift, which is generally expected to be ∼two orders of magnitude slower than isomerization that proceed through smaller transition states,[59,62] but isomerization from aldehyde H atoms is also expected to be quite fast,[59,63] thereby enabling autooxidation, which has been recently reported for OH−akane oxidation chemistry.[60]

Second-generation oxidation of ring-opened BCH molecules is likely and is also illustrated in part in Scheme 2. H-abstraction is expected to occur rapidly at an aldehyde carbon such as in structure 2 in Scheme 3[29] to produce an acyl radical that will fragment or react with O_2 to form an acyl peroxy radical. In the absence of NO_x, the acyl peroxy radical can undergo isomerization,[58,64] react with HO_2 to form a carboxylic acid, a peroxy acid, or an acyloxy radical,[49] or potentially react with RO_2. The chemistry of the acyl peroxy radical in a similar system, ring-opened cyclohexene, has also been discussed in recent work.[64] The rate at which the acyl peroxy radical (2-AOO) isomerizes, k_2, is predicted to be relatively fast[58,59] at ∼0.5 s^{-1} based on estimations via structure−activity relationships.[59] Acyloxy radicals formed in this step will likely undergo fragmentation to produce CO_2 and a primary alkyl radical,[51] which will then continue to produce RO_2 and/or RO in subsequent reactions (not shown). This represents a clear and probable pathway toward forming carboxylic and peroxy acids during BCH oxidation. An increased propensity for particle-phase organic acid formation during BCH oxidation compared to decane oxidation is reflected in the ACSM data (Table 1) with significantly higher ACSM f_{44} values for BCH (∼0.11) than for decane (∼0.07) under low-NO_x conditions. f_{44} is the fraction of the organic signal at m/z 44, which is attributed primarily to CO_2^+ and

https://doi.org/10.1021/acs.jpca.1c03516
J. Phys. Chem. A XXXX, XXX, XXX−XXX

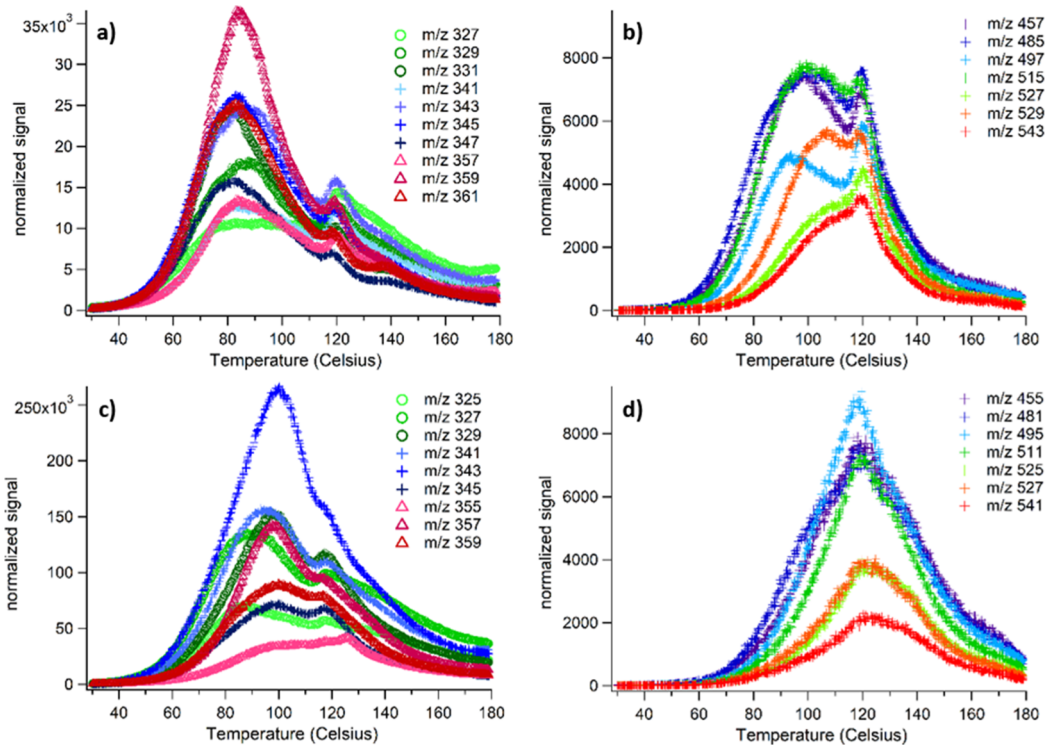

Figure 4. Thermogram desorption profiles for monomers (a,c) and oligomers/dimers (b,d) for SOA from decane [(a,b) expt. 6] and BCH [(c,d) expt. 11], both conducted under low NO_x and medium RH. Note the difference in *y*-axis scale between (a,c) but not (b,d). In (a,c), green symbols correspond primarily to $C_{10}H_{14-20}O_4I$, blue symbols to $C_{10}H_{14-20}O_5I$, and red symbols to $C_{10}H_{12-18}O_6I$. In (b,d), the *m*/*z* correspond to a mixture of multifunctional oligomeric (C_{10-20}) and dimeric (C_{20}) molecules.

assumed to mostly originate from carboxylic acids.[65] Differing amounts of organic acids in decane and BCH SOA may affect particle-phase processes such as oligomerization and other heterogeneous reactions.[49]

The reaction pathways illustrated in Scheme 3 for the low-NO_x oxidation of BCH rely on the reaction between two RO_2 radicals to form RO radicals, though RO may also form due to reaction with Cl.[42] Photolysis of ROOH may also form RO in environmental systems and some chamber experiments;[38,66] however, based on the 354 nm wavelength lights used in this work, we suspect that gas-phase photolysis of ROOH does not occur to a significant extent in the present work.[67] RO_2-RO_2 and RO_2-Cl (or RO_2-OH) reactions may be of limited significance in atmospheric systems[40] but may occur in the low-NO_x experiments described here. Chamber modeling (see Supporting Information, Section S1) shows that the concentration of Cl atoms, [Cl], is initially 2.6×10^7 molecules cm^{-3}, about 40 times lower than $[HO_2]$ (approximately 1.0×10^9 molecules cm^{-3}), suggesting that RO_2-Cl reactions may occur but will not be a substantial RO_2 loss process.[40] The rapid oxidation of alkanes by Cl[3,4] will lead to a high $[RO_2]$ (approximately 6.5×10^{10} molecules cm^{-3}) and fast multigenerational chemistry (as discussed in Section 3.1 and in prior work[1]). RO_2-RO_2 reactions have rate constants that vary considerably depending on RO_2 structure and substitution and are generally lower than those for HO_2-RO_2,[40,49,68] but RO_2-RO_2 reactions may be competitive immediately after alkane oxidation begins when $[HO_2]$ is low or over the first several minutes of alkane oxidation when multigenerational chemistry may lead to the formation of substituted peroxy radicals.[68] In atmospheric regimes where RO_2 + HO_2 chemistry is more dominant, the formation of hydroperoxy and carbonyl groups is expected to be most favorable and ring opening resulting directly from gas-phase oxidation may not occur to a significant extent. Photolysis or heterogeneous reactions may still lead to ring opening as molecules persist in the atmosphere.[38,66]

3.3. Particle-Phase Differences between BCH and Decane SOA. Previous work has shown that multifunctional nitrates present as monomer and oligomeric molecules are significant components of SOA formed from Cl oxidation of linear alkanes under high-NO_x conditions.[1] We expect BCH SOA formed under high-NO_x to have a similar overall composition compared to decane, as chemistry proceeds similarly for the molecules following ring opening in BCH. FIGAERO-CIMS analysis of decane and BCH SOA produced under low-NO_x, medium RH conditions (exps 6 and 11 in Table 1) shows that the most common compounds are C10 molecules (monomers) and that oligomeric compounds are also present to a significant extent (Figures 3 and 4). Average mass spectra for the FIGAERO desorption thermograms for BCH and decane are shown in Figure 3. Peak clusters corresponding to specific $C_xH_yO_z$ families are indicated on the mass spectrum. Comparison between decane and BCH peaks shows that similar $C_xH_yO_z$ families are represented in the SOA of both compounds, though many of the most intense monomer peaks (Figure 3a) in the BCH spectrum are shifted 2 *m*/*z* lower than in decane. This reflects the 2 fewer H that are present in the parent BCH structure ($C_{10}H_{20}$) compared to decane ($C_{10}H_{22}$) and suggests the preservation of the ring structure in many condensed phase molecules. Dimer and larger oligomer peaks (Figure 3b) in the BCH spectrum are shifted lower by 4 *m*/*z*, while smaller oligomer peaks are shifted lower by 2 *m*/*z*, reflecting the presence of both ring-retaining and ring-opened molecules.

https://doi.org/10.1021/acs.jpca.1c03516
J. Phys. Chem. A XXXX, XXX, XXX−XXX

A comparison of the temperature-dependent FIGAERO thermogram signals for several of the most common monomer compounds are shown in Figure 4. Most BCH oxidation products desorb at higher temperatures than their decane counterparts with similar molecular formula, with the temperature at which maximum signal intensity is reached (T_{max}) differing by 5−20 °C. We do not believe that these T_{max} values are significantly affected by filter loading artifacts, as filter loadings are comparable and are calculated to be above those at which T_{max} shifts were observed to plateau in prior work.[1,69] This indicates that BCH monomers have lower volatilities, which could arise from two factors. First, BCH oxidation products that retain the ring structure will have an inherently lower vapor pressure due to the presence of functional groups on the ring structure.[31,32] Second, ring-opened BCH oxidation products will contain terminal functional groups that lower the vapor pressure of a molecule more than non-terminal functional groups.[31,32] We suspect that preservation of the ring structure more strongly contributes to the observed T_{max} differences based on the previously mentioned 2 m/z difference between the most intense peaks in the decane and BCH spectra (Figure 4) as well as a comparison of thermograms for high-NO_x BCH and decane SOA, as shown in Figure S6. Under high-NO_x conditions, the thermogram profiles and T_{max} for non-nitrate BCH and decane monomers are more similar. High-NO_x conditions will favor RO chemistry and lead to more ring opening occurring during BCH oxidation, so fewer high-NO_x BCH oxidation products are expected to retain the ring structure.

It is also apparent from Figure 4a,c that signal for C10 molecules typically have a T_{max} of 80−100 °C but also possess a secondary maximum at higher temperatures of 120−130 °C. This secondary maximum coincides with the T_{max} for oligomeric molecules (consisting of C < 20 oligomers and C20 dimers) that are shown in Figure 4b,d, suggesting that the secondary desorption maximum is due to thermal breakdown of oligomers and dimers.[1,47] Some C < 20 oligomeric signals (Figure 4b,d) also have a primary and secondary T_{max}. This may reflect different structures with the same formula or could result from the thermal breakdown of larger oligomers that leads to the volatilization of a portion of the parent oligomer. Oligomer and dimer signals compose a smaller fraction of BCH SOA than decane SOA, as shown in Figure 3b. This indicates that a smaller fraction of BCH SOA is composed of oligomeric molecules, which maybe be due to increased thermal decomposition of BCH oligomers or a lower BCH dimer production rate. Previous work theorized that thermal fragmentation begins to dominate over evaporation at temperatures near ∼120 °C for alkane−Cl SOA,[1] which is the temperature range where most decane dimers reach T_{max} (Figure 4). Since BCH monomers typically have a higher T_{max} than decane monomers, BCH dimers may also have higher T_{max} than decane dimers. BCH dimers would therefore be more likely to thermally decompose before volatilizing, given the ∼120 °C high-temperature limit for analyzing the thermal desorption of alkane−Cl SOA.[1] However, C < 20 oligomer and dimer signals that peak well before 120 °C (e.g., those near m/z 457, 485, 497, and 515) in decane SOA are also less intense in BCH SOA, as seen in Figure 3b. C < 10 fragmentation products that form during alkane oxidation serve as precursors (in addition to C10 monomers) for C < 20 oligomers. Fragmentation products can form during second-generation, and later oxidation of either decane or BCH after functional groups has been added to the parent molecule.[28,33] Depending on the location at which H-abstraction occurs in BCH, fragmentation may be less likely because of the ring structure or may be more likely because of the branching points in the molecule, as was observed in prior work.[37]

The lower abundance of oligomers formed under low-NO_x conditions from branched cycloalkane SOA compared to linear alkane SOA is consistent with past work,[70] although the exact reason for which this occurs is unclear. Molecules containing potential precursors to oligomeric compounds, including peroxy and carbonyl groups, were previously observed in branched cycloalkane SOA.[70] Ring structures can be incorporated into oligomeric molecules, as laid out in the reaction schematics of prior work;[70,71] however, such oligomers may not necessarily be stable. Six-membered rings are generally most stable when functional groups are located equatorial to the ring, as opposed to axial, but if oligomerization reactions occur between functional groups on a cyclohexyl ring (such as a carbonyl group in functionalized BCH), the resulting structure would have functional groups in both the axial and equatorial positions. This may destabilize the oligomer and favor the reverse reaction to individual monomers.

3.4. Trends in SOA Production. ACSM-derived values for SOA yield and fractional values for selected organic ions for each experiment are listed in Table 1. f_{43} represents the fraction of the total organic signal observed at m/z 43 and is attributed primarily to $C_2H_3O^+$, while f_{44} represents the fraction of the total organic signal at m/z 44 and is attributed primarily to CO_2^+.[65] Several trends are visible across the experimental data. Under high-NO_x and low-RH conditions, SOA production decreases on the order BCH > decane > 2-MeNo > 3,3-DMO, following the trend of decreasing SOA with increasing degree of branching that has been observed in prior work for OH-initiated chemistry.[36,37,72] An increased degree of branching increases the relative amount of alkoxy radical intermediates that decompose, as fragmentation to produce a secondary or tertiary carbon radical is more favorable than production of a primary carbon radical. Fragmentation produces two molecules of higher volatility than the parent molecule, thereby decreasing the potential for SOA formation in the system. These fragmentation products must undergo further oxidation in order to condense to the particle phase, which increases the oxidized character of SOA derived from branched alkanes and is consistent with the increased f_{44} values for 2-MeNo and 3,3-DMO relative to decane (Table 1). Alkoxy radical decomposition and fragmentation of BCH can be favorable if H-abstraction occurs on the butyl substituent α to the ring, but decomposition of an alkoxy radical located on the ring results in a ring-opening process rather than molecular fragmentation, thereby preserving the C10 structure. ACSM measurements suggests a differing oxidized character for SOA from BCH and decane, based on lower f_{43} values for BCH SOA across all conditions and comparable or higher f_{44} values for BCH SOA under high-NO_x and low-NO_x conditions, respectively. Lower f_{43} values indicate a lower oxidized organic character[65] and may originate from ring-retaining BCH molecules, discussed in Section 3.3, that require a lesser degree of oxidation than decane to reach sufficiently low vapor pressure and condense to the particle phase. Higher f_{44} values likely result from ring-opened BCH reactions that form organic acids[65] under low-NO_x conditions, as discussed in Section 3.2.

https://doi.org/10.1021/acs.jpca.1c03516
J. Phys. Chem. A XXXX, XXX, XXX−XXX

More SOA is produced from decane and BCH oxidation under low-NO_x compared to high-NO_x conditions. Additionally, BCH tends to produce more SOA than decane under low-NO_x conditions, in particular at low RH. Increasing RH (to values in the range ~40−55%) decreases SOA production under high NO_x for decane but in the absence of NOx, it increases SOA yield for decane and has no apparent impact on SOA yield for BCH. Low-NO_x conditions favor peroxy radical (RO_2) chemistry over alkoxy radical (RO) chemistry. More prevalent RO chemistry may enhance SOA formation from alkanes by enabling the rapid addition of multiple functional groups to molecules through alkoxy radical isomerization[50,55] and subsequent multi-generational chemistry.[35,36] Under high NO_x conditions, increased RO chemistry is expected to lead to more molecular fragmentation[35,36,50] and NO_2 may scavenge radical oxidants,[1] thereby reducing SOA formed. Elevated RH can have mixed effects on SOA formation[73] and has previously been observed to suppress oligomer formation[70] and acid-catalyzed reactions,[74] but the formation of HCl and organic acids during our experiments may lower aerosol pH and facilitate acid-catalyzed processes. The differing effects of RH on low-NO_x decane and BCH SOA may relate to the compositional differences discussed in Section 3.3 or may be due to other factors. Effects of RH on SOA formation and composition may also become more pronounced during longer timescales than the present experiments.

The trend of reduced SOA formation under high-NO_x conditions for linear and branched cycloalkanes is consistent with recent work with OH[27] and in contrast to other prior work with OH.[72] Differences compared to past work may occur due to differing oxidant exposure and aging timescales. In the present work and in the work of Li et al. (2019),[27] who used an oxidation flow reactor, SOA production was measured after a relatively short but intense oxidant exposure timescale of 2 min, compared to 20−25 min in this work. The experiments of Loza et al. (2014) measured SOA production after a period of several hours of UV and less-intense oxidant exposure.[72] Less-intense oxidant exposure may increase SOA yield under high-NO_x conditions through the addition of more functional groups to parent VOCs via alkoxy radical chemistry (relative to low-NO_x) and by limiting the extent to which fragmentation reactions occur (relative to higher oxidant exposure). Under low-NO_x conditions, a longer UV exposure and aging timescale may enable increased photolysis of hydroperoxy and/or carbonyl molecules,[66] leading to more fragmentation and less SOA. Different concentrations of RO_2 and HO_2 radicals formed may also affect how oxidation proceeds and terminates. The differing observations on SOA formation between these works suggest that high-NO_x and low-NO_x alkane-derived SOA undergo chemical aging along different timescales and potentially through different mechanisms.

RO_2-centric autoxidation reactions forming highly oxidized molecules (HOMs) have seen recent attention as a mechanism by which SOA can form (primarily in biogenic systems) under low-NO_x conditions[75] and potentially under high-NO_x conditions as well.[60] Molecules with a high number of oxygen atoms (non-nitrate O/C $\geq$ 0.5) are detected in the particle phase during FIGAERO desorption measurements of SOA formed from decane and BCH under high- and low-NO_x conditions (Figures 3 and S5; see also Wang and Hildebrandt Ruiz, 2018), consistent with recent work on OH-initiated alkane oxidation.[60] However, our data do not provide definitive evidence for or against the formation of autoxidation-derived molecules in the present work.[60,75,76] Several different mechanisms, some of which involve auto-oxidation, could explain the observed high oxygen number molecules. High-NO_x conditions can enable the addition of multiple functional groups to an alkane through RO isomerization and subsequent chemistry during a single generation of oxidation, as described previously.[35,60] Although autoxidation reactions of simple hydrocarbons are generally expected to terminate quickly,[75] the formation of aldehyde groups through the abstraction of primary H or ring opening in BCH may provide avenues by which autoxidation reactions can occur.[60,64,75] Such reactions may proceed, for example, via abstraction of an aldehyde H by a peroxy radical[59,63] or via acyl peroxy radicals[58,59] that are generated following abstraction of an aldehyde H. Overall, though we cannot say with certainty, autoxidation processes may contribute to the increase in SOA production under low-NO_x conditions observed in this work and to trends in SOA production by Cl oxidation more generally.[1]

Previous studies have shown that the net effects of NO_x on SOA formation depend on the structure of the hydrocarbon precursors, hydrocarbon/NO_x ratio,[27,37,70,72,73] and NO_x speciation. Prior work with C8−C12 linear alkanes showed that experiments with a higher initial NO/NO_2 ratio produced more SOA.[1] The decrease in SOA formed under elevated RH and high NO_x was discussed in greater detail in prior work[1] and is consistent with recent work on OH-derived alkane SOA,[77] where decreased SOA production was attributed to inhibition of the acid-catalyzed cyclization of 1,4-hydroxycarbonyl molecules.[74,77] Fewer 1,4-hydroxycarbonyl molecules are expected to form under low-NO_x conditions where RO_2 chemistry is favored,[49,74] so the impact of RH between low- and high-NO_x conditions is not expected to be directly analogous. RH has been observed to both enhance and suppress SOA formation[70,73] and would be expected to primarily affect particle-phase processes such as heterogeneous chemical reactions, oligomerization,[49] and organonitrate hydrolysis.[78,79] Aerosol pH may affect these processes but was not investigated in this work. However, HCl produced through gas-phase and heterogeneous H-abstraction[80] by Cl may interact with particles and particle surfaces to affect heterogeneous processes. The formation of organic acids following primary H abstraction or ring opening in BCH may also be able to catalyze some particle-phase processes.[49]

4. SIGNIFICANCE AND IMPLICATIONS

Our experiments on the oxidation of C10 alkanes by Cl show that, compared to a base scenario with a linear alkane, SOA formation is lower for a branched parent alkane and higher for a branched cycloalkane; these observations are similar to conclusions of prior work using OH.[35−38] Molecular fragmentation products detected during the oxidation of 3,3-DMO are consistent with the abstraction of primary H by Cl, which confirms prior theory[3] and is an expected mechanistic difference between Cl and OH oxidation of medium- and long-chain alkanes. When comparing the initial oxidation of alkanes with uniform carbon number, the oxidation of branched alkanes by Cl likely differs most significantly from oxidation by OH due to a higher percentage of total H being primary, primary-adjacent, or tertiary, though whether this leads to significant differences in SOA production will depend on how substituent length and location within the larger alkyl structure

https://doi.org/10.1021/acs.jpca.1c03516
J. Phys. Chem. A XXXX, XXX, XXX−XXX

impact secondary radical (RO, RO_2) propagation and termination.[28,33,34] Primary H abstraction enables the formation of primary functional groups (such as organic acids and PANs, as well as nitrates, alcohols, and aldehydes) during alkane oxidation without proceeding through RO decomposition or multi-generational heterogeneous chemistry. This leads to increased production of high-carbon number organic acids (under low NO_x conditions) or PANs (under high NO_x conditions) when Cl is present to participate in oxidation chemistry. The production of primary alcohols and nitrates will likely lead to more SOA production during later-generation chemistry,[28,33] while the production of aldehydes that may ultimately lead to increased fragmentation or participate in autoxidation will likely lead to overall more varied chemistry compared to what is observed in OH-only systems.

BCH and decane oxidation products possess similar molecular formulae under both low-NO_x and high-NO_x conditions and the high-NO_x SOA properties appear to be similar. However, oxidation under low-NO_x conditions leads to several differences in the molecular-level properties between decane and BCH SOA that relate to the behavior of the BCH hexyl ring. First, low-NO_x BCH oxidation products are generally of lower volatility than those of decane, which likely results from molecules that retain the hexyl ring[31,32] and contribute to increased SOA formation from BCH under low-NO_x conditions. Second, oligomerization occurs to a lesser extent in low-NO_x BCH SOA, which is consistent with past work[70] and may result from steric hindrances to oligomerization for ring-retaining molecules. Third, ring-opened BCH molecules lead to increased formation of organic peroxy and carboxylic acids, as evidenced by higher f_{44} values for low-NO_x BCH SOA. These molecular-level differences between the oxidation products of branched cycloalkanes and linear alkanes may lead to differences in SOA formation and properties and how SOA evolves during atmospheric chemical aging.

Oxidation of *n*-alkanes by Cl was previously observed to differ from oxidation by OH through a more rapid reaction timescale and an increase in SOA yield.[1] The present work suggests that similar trends also hold for alkanes of varying structures. These differences likely arise, in part, from differences in where Cl and OH abstract H on the carbon backbone (Table 2) and how this affects multigenerational chemistry. SOA formation following initial oxidation is controlled, in part, by the activating and deactivating effects of different functional groups towards H-abstraction during internal isomerization and second-generation chemistry.[28,33,34] Significantly, molecules with functional groups on primary or primary-adjacent carbons (the locations where Cl is more likely to abstract H compared to OH) tend to undergo less fragmentation and therefore produce more SOA during multigenerational chemistry.[28,33,34] A survey of the available literature[18] suggests that there are also some potentially significant differences in substituent effects between H-abstraction by Cl and by OH. Prior work examining Cl oxidation of linear, branched, and cycloalkanes observed alkyl substituents to have a deactivating effect on oxidation by Cl, in contrast to oxidation by OH.[3] Cl also reacts more quickly with several linear alkanes than their counterparts with oxygen-containing functional groups, a trend which is generally opposite that of OH.[18] This trend is especially true for aldehydes, which are greatly activated toward reaction with OH but tend to react more slowly with Cl.[18] These differences likely arise for multiple reasons, but overall suggest less specificity for H-abstraction by Cl towards functionalized alkanes, particularly aldehydes, and demonstrate the need for more complete structure activity relationships to predict alkane−Cl reactivity.[3,81] Less specificity by Cl when oxidizing hydroxyl- and aldehyde-substituted alkanes may also lead to a decrease in molecular fragmentation[33,51] and a corresponding increase in SOA production, following in the "functionalization vs fragmentation" framework for VOC oxidation.[82] However, further work would be needed to determine the extent to which Cl and OH reactivity trends differ in functionalized and multifunctional molecules and potential effects on SOA formation.

■ ASSOCIATED CONTENT

Supporting Information

The Supporting Information is available free of charge at https://pubs.acs.org/doi/10.1021/acs.jpca.1c03516.

Description of the chamber modeling work and site-specific hydrogen abstraction ratio calculations, and figures and reaction schemes (PDF)

■ AUTHOR INFORMATION

Corresponding Author

Lea Hildebrandt Ruiz − *McKetta Department of Chemical Engineering, The University of Texas at Austin, Austin 78712 Texas, United States;* orcid.org/0000-0001-8378-1882; Email: lhr@che.utexas.edu

Authors

Leif G. Jahn − *McKetta Department of Chemical Engineering, The University of Texas at Austin, Austin 78712 Texas, United States;* orcid.org/0000-0002-5616-4448

Dongyu S. Wang − *McKetta Department of Chemical Engineering, The University of Texas at Austin, Austin 78712 Texas, United States; Now at Laboratory of Atmospheric Chemistry, Paul Scherrer Institute, 5232 Villigen, Switzerland*

Surya Venkatesh Dhulipala − *McKetta Department of Chemical Engineering, The University of Texas at Austin, Austin 78712 Texas, United States; Now at Department of Mechanical Engineering, The University of British Columbia, V6T 1Z4 Vancouver, Canada*

Complete contact information is available at: https://pubs.acs.org/10.1021/acs.jpca.1c03516

Notes

The authors declare no competing financial interest.

■ ACKNOWLEDGMENTS

This material is based upon work supported in part by the National Science Foundation under grant no. 1653625 and the Welch Foundation under grants no. F-1925-20170325 and F-1925-20200401. L.G.J. was supported by the Camille and Henry Dreyfus Foundation Postdoctoral Program in Environmental Chemistry. We thank all sponsors for their generous support. We thank Mrinali Modi for modeling the chamber experiments.

■ REFERENCES

(1) Wang, D. S.; Hildebrandt Ruiz, L. Chlorine-Initiated Oxidation of n-Alkanes under High-NOx Conditions: Insights into Secondary Organic Aerosol Composition and Volatility Using a FIGAERO−CIMS. *Atmos. Chem. Phys.* **2018**, *18*, 15535−15553.

(2) Saiz-Lopez, A.; von Glasow, R. Reactive Halogen Chemistry in the Troposphere. *Chem. Soc. Rev.* **2012**, *41*, 6448−6472.
(3) Aschmann, S. M.; Atkinson, R. Rate Constants for the Gas-Phase Reactions of Alkanes with Cl Atoms at 296 ± 2 K. *Int. J. Chem. Kinet.* **1995**, *27*, 613−622.
(4) Atkinson, R.; Baulch, D. L.; Cox, R. A.; Crowley, J. N.; Hampson, R. F.; Hynes, R. G.; Jenkin, M. E.; Rossi, M. J.; Troe, J. Evaluated Kinetic and Photochemical Data for Atmospheric Chemistry: Volume II − Gas Phase Reactions of Organic Species. *Atmos. Chem. Phys.* **2006**, *6*, 3625−4055.
(5) Faxon, C. B.; Allen, D. T. Chlorine Chemistry in Urban Atmospheres: A Review. *Environ. Chem.* **2013**, *10*, 221.
(6) Finlayson-Pitts, B. J. The Tropospheric Chemistry of Sea Salt: A Molecular-Level View of the Chemistry of NaCl and NaBr. *Chem. Rev.* **2003**, *103*, 4801−4822.
(7) Faxon, C.; Bean, J.; Ruiz, L. Inland Concentrations of Cl2 and ClNO2 in Southeast Texas Suggest Chlorine Chemistry Significantly Contributes to Atmospheric Reactivity. *Atmosphere* **2015**, *6*, 1487−1506.
(8) Faxon, C. B.; Dhulipala, S. V.; Allen, D. T.; Hildebrandt Ruiz, L. Heterogeneous Production of Cl2 from Particulate Chloride: Effects of Composition and Relative Humidity. *AIChE J.* **2018**, *64*, 3151−3158.
(9) Tham, Y. J.; Wang, Z.; Li, Q.; Yun, H.; Wang, W.; Wang, X.; Xue, L.; Lu, K.; Ma, N.; Bohn, B.; et al. Significant Concentrations of Nitryl Chloride Sustained in the Morning: Investigations of the Causes and Impacts on Ozone Production in a Polluted Region of Northern China. *Atmos. Chem. Phys.* **2016**, *16*, 14959−14977.
(10) Thornton, J. A.; Kercher, J. P.; Riedel, T. P.; Wagner, N. L.; Cozic, J.; Holloway, J. S.; Dubé, W. P.; Wolfe, G. M.; Quinn, P. K.; Middlebrook, A. M.; et al. A Large Atomic Chlorine Source Inferred from Mid-Continental Reactive Nitrogen Chemistry. *Nature* **2010**, *464*, 271−274.
(11) Ahern, A. T.; Goldberger, L.; Jahl, L.; Thornton, J.; Sullivan, R. C. Production of N2O5 and ClNO2 through Nocturnal Processing of Biomass-Burning Aerosol. *Environ. Sci. Technol.* **2018**, *52*, 550−559.
(12) Goldberger, L. A.; Jahl, L. G.; Thornton, J. A.; Sullivan, R. C. N2O5 Reactive Uptake Kinetics and Chlorine Activation on Authentic Biomass-Burning Aerosol. *Environ. Sci.: Processes Impacts* **2019**, *21*, 1684−1698.
(13) Mitroo, D.; Gill, T. E.; Haas, S.; Pratt, K. A.; Gaston, C. J. ClNO2 Production from N2O5 Uptake on Saline Playa Dusts: New Insights into Potential Inland Sources of ClNO2. *Environ. Sci. Technol.* **2019**, *53*, 7442−7452.
(14) McNamara, S. M.; Kolesar, K. R.; Wang, S.; Kirpes, R. M.; May, N. W.; Gunsch, M. J.; Cook, R. D.; Fuentes, J. D.; Hornbrook, R. S.; Apel, E. C.; et al. Observation of Road Salt Aerosol Driving Inland Wintertime Atmospheric Chlorine Chemistry. *ACS Cent. Sci.* **2020**, *6*, 684−694.
(15) Wang, X.; Jacob, D. J.; Fu, X.; Wang, T.; Breton, M. L.; Hallquist, M.; Liu, Z.; McDuffie, E. E.; Liao, H. Effects of Anthropogenic Chlorine on PM 2.5 and Ozone Air Quality in China. *Environ. Sci. Technol.* **2020**, *54*, 9908−9916.
(16) Wang, D. S.; Ruiz, L. H. Secondary Organic Aerosol from Chlorine-Initiated Oxidation of Isoprene. *Atmos. Chem. Phys.* **2017**, *17*, 13491−13508.
(17) Dhulipala, S. V.; Bhandari, S.; Hildebrandt Ruiz, L. Formation of Oxidized Organic Compounds from Cl-Initiated Oxidation of Toluene. *Atmos. Environ.* **2019**, *199*, 265−273.
(18) McGillen, M. R.; Carter, W. P. L.; Mellouki, A.; Orlando, J. J.; Picquet-Varrault, B.; Wallington, T. J. Database for the Kinetics of the Gas-Phase Atmospheric Reactions of Organic Compounds. *Earth Syst. Sci. Data* **2020**, *12*, 1203−1216.
(19) Gentner, D. R.; Jathar, S. H.; Gordon, T. D.; Bahreini, R.; Day, D. A.; El Haddad, I.; Hayes, P. L.; Pieber, S. M.; Platt, S. M.; de Gouw, J.; et al. Review of Urban Secondary Organic Aerosol Formation from Gasoline and Diesel Motor Vehicle Emissions. *Environ. Sci. Technol.* **2017**, *51*, 1074−1093.
(20) Caravaggio, G. A.; Charland, J.-P.; Macdonald, P.; Graham, L. N -Alkane Profiles of Engine Lubricating Oil and Particulate Matter by Molecular Sieve Extraction. *Environ. Sci. Technol.* **2007**, *41*, 3697−3701.
(21) Kleeman, M. J.; Riddle, S. G.; Robert, M. A.; Jakober, C. A. Lubricating Oil and Fuel Contributions To Particulate Matter Emissions from Light-Duty Gasoline and Heavy-Duty Diesel Vehicles. *Environ. Sci. Technol.* **2008**, *42*, 235−242.
(22) Khare, P.; Machesky, J.; Soto, R.; He, M.; Presto, A. A.; Gentner, D. R. Asphalt-Related Emissions Are a Major Missing Nontraditional Source of Secondary Organic Aerosol Precursors. *Sci. Adv.* **2020**, *6*, No. eabb9785.
(23) McDonald, B. C.; De Gouw, J. A.; Gilman, J. B.; Jathar, S. H.; Akherati, A.; Cappa, C. D.; Jimenez, J. L.; Lee-Taylor, J.; Hayes, P. L.; McKeen, S. A.; et al. Volatile Chemical Products Emerging as Largest Petrochemical Source of Urban Organic Emissions. *Science* **2018**, *359*, 760−764.
(24) Khare, P.; Gentner, D. R. Considering the Future of Anthropogenic Gas-Phase Organic Compound Emissions and the Increasing Influence of Non-Combustion Sources on Urban Air Quality. *Atmos. Chem. Phys. Discuss.* **2017**, 1−69.
(25) Swarthout, R. F.; Russo, R. S.; Zhou, Y.; Hart, A. H.; Sive, B. C. Volatile Organic Compound Distributions during the NACHTT Campaign at the Boulder Atmospheric Observatory: Influence of Urban and Natural Gas Sources. *J. Geophys. Res. Atmos.* **2013**, *118*, 10,614−10,637.
(26) Garcia-Gonzales, D. A.; Shonkoff, S. B. C.; Hays, J.; Jerrett, M. Hazardous Air Pollutants Associated with Upstream Oil and Natural Gas Development: A Critical Synthesis of Current Peer-Reviewed Literature. *Annu. Rev. Publ. Health* **2019**, *40*, 283−304.
(27) Li, K.; Liggio, J.; Han, C.; Liu, Q.; Moussa, S. G.; Lee, P.; Li, S.-M. Understanding the Impact of High-NOx Conditions on the Formation of Secondary Organic Aerosol in the Photooxidation of Oil Sand-Related Precursors. *Environ. Sci. Technol.* **2019**, *53*, 14420−14429.
(28) Algrim, L. B.; Ziemann, P. J. Effect of the Nitrate Group on Yields and Composition of Secondary Organic Aerosol Formed from Reactions of Alkyl Nitrates with OH Radicals in the Presence of NO X. *Aerosol Sci. Technol.* **2020**, *54*, 1070−1082.
(29) Kwok, E.; Atkinson, R. Estimation of Hydroxyl Radical Reaction Rate Constants for Gas-Phase Organic Compounds Using a Structure-Reactivity Relationship: An Update. *Atmos. Environ.* **1995**, *29*, 1685−1695.
(30) Carrasquillo, A. J.; Hunter, J. F.; Daumit, K. E.; Kroll, J. H. Secondary Organic Aerosol Formation via the Isolation of Individual Reactive Intermediates: Role of Alkoxy Radical Structure. *J. Phys. Chem. A* **2014**, *118*, 8807−8816.
(31) Compernolle, S.; Ceulemans, K.; Müller, J.-F. EVAPORATION: A New Vapour Pressure Estimation Methodfor Organic Molecules Including Non-Additivity and Intramolecular Interactions. *Atmos. Chem. Phys.* **2011**, *11*, 9431−9450.
(32) Pankow, J. F.; Asher, W. E. SIMPOL.1: A Simple Group Contribution Method for Predicting Vapor Pressures and Enthalpies of Vaporization of Multifunctional Organic Compounds. *Atmos. Chem. Phys.* **2008**, *8*, 2773−2796.
(33) Algrim, L. B.; Ziemann, P. J. Effect of the Hydroxyl Group on Yields and Composition of Organic Aerosol Formed from OH Radical-Initiated Reactions of Alcohols in the Presence of NOx. *ACS Earth Space Chem.* **2019**, *3*, 413−423.
(34) Algrim, L. B.; Ziemann, P. J. Effect of the Keto Group on Yields and Composition of Organic Aerosol Formed from OH Radical-Initiated Reactions of Ketones in the Presence of NOx. *J. Phys. Chem. A* **2016**, *120*, 6978−6989.
(35) Lim, Y. B.; Ziemann, P. J. Chemistry of Secondary Organic Aerosol Formation from OH Radical-Initiated Reactions of Linear, Branched, and Cyclic Alkanes in the Presence of NO X. *Aerosol Sci. Technol.* **2009**, *43*, 604−619.
(36) Lim, Y. B.; Ziemann, P. J. Effects of Molecular Structure on Aerosol Yields from OH Radical-Initiated Reactions of Linear,

https://doi.org/10.1021/acs.jpca.1c03516
J. Phys. Chem. A XXXX, XXX, XXX−XXX

Branched, and Cyclic Alkanes in the Presence of NO X. *Environ. Sci. Technol.* **2009**, *43*, 2328−2334.
(37) Hunter, J. F.; Carrasquillo, A. J.; Daumit, K. E.; Kroll, J. H. Secondary Organic Aerosol Formation from Acyclic, Monocyclic, and Polycyclic Alkanes. *Environ. Sci. Technol.* **2014**, *48*, 10227−10234.
(38) Yee, L. D.; Craven, J. S.; Loza, C. L.; Schilling, K. A.; Ng, N. L.; Canagaratna, M. R.; Ziemann, P. J.; Flagan, R. C.; Seinfeld, J. H. Effect of Chemical Structure on Secondary Organic Aerosol Formation from C12 Alkanes. *Atmos. Chem. Phys.* **2013**, *13*, 11121−11140.
(39) Young, C. J.; Washenfelder, R. A.; Edwards, P. M.; Parrish, D. D.; Gilman, J. B.; Kuster, W. C.; Mielke, L. H.; Osthoff, H. D.; Tsai, C.; Pikelnaya, O.; et al. Chlorine as a Primary Radical: Evaluation of Methods to Understand Its Role in Initiation of Oxidative Cycles. *Atmos. Chem. Phys.* **2014**, *14*, 3427−3440.
(40) Peng, Z.; Lee-Taylor, J.; Orlando, J. J.; Tyndall, G. S.; Jimenez, J. L. Organic Peroxy Radical Chemistry in Oxidation Flow Reactors and Environmental Chambers and Their Atmospheric Relevance. *Atmos. Chem. Phys.* **2019**, *19*, 813−834.
(41) Assaf, E.; Schoemaecker, C.; Vereecken, L.; Fittschen, C. Experimental and Theoretical Investigation of the Reaction of RO2 Radicals with OH Radicals: Dependence of the HO2 Yield on the Size of the Alkyl Group. *Int. J. Chem. Kinet.* **2018**, *50*, 670−680.
(42) Maricq, M. M.; Szente, J. J.; Kaiser, E. W.; Shi, J. Reaction of Chlorine Atoms with Methylperoxy and Ethylperoxy Radicals. *J. Phys. Chem.* **1994**, *98*, 2083−2089.
(43) Ng, N. L.; Herndon, S. C.; Trimborn, A.; Canagaratna, M. R.; Croteau, P. L.; Onasch, T. B.; Sueper, D.; Worsnop, D. R.; Zhang, Q.; Sun, Y. L.; et al. An Aerosol Chemical Speciation Monitor (ACSM) for Routine Monitoring of the Composition and Mass Concentrations of Ambient Aerosol. *Aerosol Sci. Technol.* **2011**, *45*, 780−794.
(44) Pathak, R. K.; Stanier, C. O.; Donahue, N. M.; Pandis, S. N. Ozonolysis of α-Pinene at Atmospherically Relevant Concentrations: Temperature Dependence of Aerosol Mass Fractions (Yields). *J. Geophys. Res. Atmos.* **2007**, *112*, D03201.
(45) Huang, Y.; Zhao, R.; Charan, S. M.; Kenseth, C. M.; Zhang, X.; Seinfeld, J. H. Unified Theory of Vapor−Wall Mass Transport in Teflon-Walled Environmental Chambers. *Environ. Sci. Technol.* **2018**, *52*, 2134−2142.
(46) Lee, B. H.; Lopez-Hilfiker, F. D.; Mohr, C.; Kurtén, T.; Worsnop, D. R.; Thornton, J. A. An Iodide-Adduct High-Resolution Time-of-Flight Chemical-Ionization Mass Spectrometer: Application to Atmospheric Inorganic and Organic Compounds. *Environ. Sci. Technol.* **2014**, *48*, 6309−6317.
(47) Lopez-Hilfiker, F. D.; Mohr, C.; Ehn, M.; Rubach, F.; Kleist, E.; Wildt, J.; Mentel, T. F.; Lutz, A.; Hallquist, M.; Worsnop, D.; et al. A Novel Method for Online Analysis of Gas and Particle Composition: Description and Evaluation of a Filter Inlet for Gases and AEROsols (FIGAERO). *Atmos. Meas. Tech.* **2014**, *7*, 983−1001.
(48) Lopez-Hilfiker, F. D.; Iyer, S.; Mohr, C.; Lee, B. H.; D'ambro, E. L.; Kurtén, T.; Thornton, J. A. Constraining the Sensitivity of Iodide Adduct Chemical Ionization Mass Spectrometry to Multifunctional Organic Molecules Using the Collision Limit and Thermodynamic Stability of Iodide Ion Adducts. *Atmos. Meas. Tech.* **2016**, *9*, 1505−1512.
(49) Ziemann, P. J.; Atkinson, R. Kinetics, Products, and Mechanisms of Secondary Organic Aerosol Formation. *Chem. Soc. Rev.* **2012**, *41*, 6582.
(50) Orlando, J. J.; Tyndall, G. S.; Wallington, T. J. The Atmospheric Chemistry of Alkoxy Radicals. *Chem. Rev.* **2003**, *103*, 4657−4690.
(51) Vereecken, L.; Peeters, J. Decomposition of Substituted Alkoxy Radicals—Part I: A Generalized Structure−Activity Relationship for Reaction Barrier Heights. *Phys. Chem. Chem. Phys.* **2009**, *11*, 9062.
(52) Sivaramakrishnan, R.; Michael, J. V. Rate Constants for OH with Selected Large Alkanes: Shock-Tube Measurements and an Improved Group Scheme. *J. Phys. Chem. A* **2009**, *113*, 5047−5060.
(53) Tyndall, G. S.; Orlando, J. J.; Wallington, T. J.; Dill, M.; Kaiser, E. W. Kinetics and Mechanisms of the Reactions of Chlorine Atoms with Ethane, Propane, and n-Butane. *Int. J. Chem. Kinet.* **1997**, *29*, 43−55.
(54) Bilde, M.; Barsanti, K.; Booth, M.; Cappa, C. D.; Donahue, N. M.; Emanuelsson, E. U.; McFiggans, G.; Krieger, U. K.; Marcolli, C.; Topping, D.; et al. Saturation Vapor Pressures and Transition Enthalpies of Low-Volatility Organic Molecules of Atmospheric Relevance: From Dicarboxylic Acids to Complex Mixtures. *Chem. Rev.* **2015**, *115*, 4115−4156.
(55) Vereecken, L.; Peeters, J. A Structure-Activity Relationship for the Rate Coefficient of H-Migration in Substituted Alkoxy Radicals. *Phys. Chem. Chem. Phys.* **2010**, *12*, 12608−12620.
(56) Calvert, J. G.; Derwent, R. G.; Orlando, J. J.; Tyndall, G. S.; Wallington, T. J. *Mechanisms of Atmospheric Oxidation of the Alkanes*; Oxford University Press, Incorporated: Cary, United States, 2008.
(57) Méreau, R.; Rayez, M.-T.; Rayez, J.-C.; Caralp, F.; Lesclaux, R. Theoretical Study on the Atmospheric Fate of Carbonyl Radicals: Kinetics of Decomposition Reactions. *Phys. Chem. Chem. Phys.* **2001**, *3*, 4712.
(58) Knap, H. C.; Jørgensen, S. Rapid Hydrogen Shift Reactions in Acyl Peroxy Radicals. *J. Phys. Chem. A* **2017**, *121*, 1470−1479.
(59) Vereecken, L.; Nozière, B. H migration in peroxy radicals under atmospheric conditions. *Atmos. Chem. Phys.* **2020**, *20*, 7429−7458.
(60) Wang, Z.; Ehn, M.; Rissanen, M. P.; Garmash, O.; Quéléver, L.; Xing, L.; Monge-Palacios, M.; Rantala, P.; Donahue, N. M.; Berndt, T.; et al. Efficient Alkane Oxidation under Combustion Engine and Atmospheric Conditions. *Commun. Chem.* **2021**, *4*, 18.
(61) Jenkin, M. E.; Valorso, R.; Aumont, B.; Rickard, A. R. Estimation of Rate Coefficients and Branching Ratios for Reactions of Organic Peroxy Radicals for Use in Automated Mechanism Construction. *Atmos. Chem. Phys.* **2019**, *19*, 7691−7717.
(62) Otkjær, R. V.; Jakobsen, H. H.; Tram, C. M.; Kjaergaard, H. G. Calculated Hydrogen Shift Rate Constants in Substituted Alkyl Peroxy Radicals. *J. Phys. Chem. A* **2018**, *122*, 8665−8673.
(63) Møller, K. H.; Bates, K. H.; Kjaergaard, H. G. The Importance of Peroxy Radical Hydrogen-Shift Reactions in Atmospheric Isoprene Oxidation. *J. Phys. Chem. A* **2019**, *123*, 920−932.
(64) Rissanen, M. P. NO2 Suppression of Autoxidation-Inhibition of Gas-Phase Highly Oxidized Dimer Product Formation. *ACS Earth Space Chem.* **2018**, *2*, 1211−1219.
(65) Canagaratna, M. R.; Jimenez, J. L.; Kroll, J. H.; Chen, Q.; Kessler, S. H.; Massoli, P.; Hildebrandt Ruiz, L.; Fortner, E.; Williams, L. R.; Wilson, K. R.; et al. Elemental Ratio Measurements of Organic Compounds Using Aerosol Mass Spectrometry: Characterization, Improved Calibration, and Implications. *Atmos. Chem. Phys.* **2015**, *15*, 253−272.
(66) Krapf, M.; El Haddad, I.; Bruns, E. A.; Molteni, U.; Daellenbach, K. R.; Prévôt, A. S. H.; Baltensperger, U.; Dommen, J. Labile Peroxides in Secondary Organic Aerosol. *Chem* **2016**, *1*, 603−616.
(67) McGillen, M. R.; Curchod, B. F. E.; Chhantyal-Pun, R.; Beames, J. M.; Watson, N.; Khan, M. A. H.; McMahon, L.; Shallcross, D. E.; Orr-Ewing, A. J. Criegee Intermediate-Alcohol Reactions, A Potential Source of Functionalized Hydroperoxides in the Atmosphere. *ACS Earth Space Chem.* **2017**, *1*, 664−672.
(68) Orlando, J. J.; Tyndall, G. S. Laboratory Studies of Organic Peroxy Radical Chemistry: An Overview with Emphasis on Recent Issues of Atmospheric Significance. *Chem. Soc. Rev.* **2012**, *41*, 6294.
(69) Huang, W.; Saathoff, H.; Pajunoja, A.; Shen, X.; Naumann, K.-H.; Wagner, R.; Virtanen, A.; Leisner, T.; Mohr, C. Alpha-Pinene Secondary Organic Aerosol at Low Temperature: Chemical Composition and Implications for Particle Viscosity. *Atmos. Chem. Phys.* **2018**, *18*, 2883−2898.
(70) Schilling Fahnestock, K. A.; Yee, L. D.; Loza, C. L.; Coggon, M. M.; Schwantes, R.; Zhang, X.; Dalleska, N. F.; Seinfeld, J. H. Secondary Organic Aerosol Composition from C12 Alkanes. *J. Phys. Chem. A* **2015**, *119*, 4281−4297.
(71) Aimanant, S.; Ziemann, P. J. Chemical Mechanisms of Aging of Aerosol Formed from the Reaction of N-Pentadecane with OH

https://doi.org/10.1021/acs.jpca.1c03516
J. Phys. Chem. A XXXX, XXX, XXX−XXX

Radicals in the Presence of NOx. *Aerosol Sci. Technol.* **2013**, *47*, 979−990.
(72) Loza, C. L.; Craven, J. S.; Yee, L. D.; Coggon, M. M.; Schwantes, R. H.; Shiraiwa, M.; Zhang, X.; Schilling, K. A.; Ng, N. L.; Canagaratna, M. R.; et al. Secondary Organic Aerosol Yields of 12-Carbon Alkanes. *Atmos. Chem. Phys.* **2014**, *14*, 1423−1439.
(73) Stirnweis, L.; Marcolli, C.; Dommen, J.; Barmet, P.; Frege, C.; Platt, S. M.; Bruns, E. A.; Krapf, M.; Slowik, J. G.; Wolf, R.; et al. Assessing the Influence of NOx Concentrations and Relative Humidity on Secondary Organic Aerosol Yields from α-Pinene Photo-Oxidation through Smog Chamber Experiments and Modelling Calculations. *Atmos. Chem. Phys.* **2017**, *17*, 5035−5061.
(74) Lim, Y. B.; Ziemann, P. J. Kinetics of the Heterogeneous Conversion of 1,4-Hydroxycarbonyls to Cyclic Hemiacetals and Dihydrofurans on Organic Aerosol Particles. *Phys. Chem. Chem. Phys.* **2009**, *11*, 8029.
(75) Bianchi, F.; Kurtén, T.; Riva, M.; Mohr, C.; Rissanen, M. P.; Roldin, P.; Berndt, T.; Crounse, J. D.; Wennberg, P. O.; Mentel, T. F.; et al. Highly Oxygenated Organic Molecules (HOM) from Gas-Phase Autoxidation Involving Peroxy Radicals: A Key Contributor to Atmospheric Aerosol. *Chem. Rev.* **2019**, *119*, 3472−3509.
(76) Riva, M.; Rantala, P.; Krechmer, J. E.; Peräkylä, O.; Zhang, Y.; Heikkinen, L.; Garmash, O.; Yan, C.; Kulmala, M.; Worsnop, D.; et al. Evaluating the Performance of Five Different Chemical Ionization Techniques for Detecting Gaseous Oxygenated Organic Species. *Atmos. Meas. Tech.* **2019**, *12*, 2403−2421.
(77) Lamkaddam, H.; Gratien, A.; Pangui, E.; David, M.; Peinado, F.; Polienor, J.; Jerome, M.; Cazaunau, M.; Gaimoz, C.; Picquet-Varrault, B.; et al. Role of Relative Humidity in the Secondary Organic Aerosol Formation from High-NOx Photooxidation of Long-Chain Alkanes: N -Dodecane Case Study. *ACS Earth Space Chem.* **2020**, *4*, 2414.
(78) Zare, A.; Fahey, K. M.; Sarwar, G.; Cohen, R. C.; Pye, H. O. T. Vapor-Pressure Pathways Initiate but Hydrolysis Products Dominate the Aerosol Estimated from Organic Nitrates. *ACS Earth Space Chem.* **2019**, *3*, 1426−1437.
(79) Takeuchi, M.; Ng, N. L. Chemical Composition and Hydrolysis of Organic Nitrate Aerosol Formed from Hydroxyl and Nitrate Radical Oxidation of Alpha-Pinene and Beta-Pinene. *Atmos. Chem. Phys.* **2019**, *19*, 12749−12766.
(80) George, I. J.; Abbatt, J. P. D. Heterogeneous Oxidation of Atmospheric Aerosol Particles by Gas-Phase Radicals. *Nat. Chem.* **2010**, *2*, 713−722.
(81) Aschmann, S. M.; Atkinson, R. Rate Constants for the Reactions of Cl Atoms with a Series of C6-C10 Cycloalkanes and Cycloketones at 297 ± 2 K. *Int. J. Chem. Kinet.* **2013**, *45*, 52−58.
(82) Kroll, J. H.; Smith, J. D.; Che, D. L.; Kessler, S. H.; Worsnop, D. R.; Wilson, K. R. Measurement of Fragmentation and Functionalization Pathways in the Heterogeneous Oxidation of Oxidized Organic Aerosol. *Phys. Chem. Chem. Phys.* **2009**, *11*, 8005.

https://doi.org/10.1021/acs.jpca.1c03516
J. Phys. Chem. A XXXX, XXX, XXX−XXX